CHINESE OPTICS LETTERS

Vol. 21, No. 6 | June 2023

Compact *in situ* microscope for photoelectron spectroscopy via two-mirror reflection

Chenyang Yue (岳晨阳)[1,2,3], Hong Jiang (江 虹)[1], Tianzhi Li (李天植)[1,4], Siyan Yao (姚思研)[1,2], Shengyue Zeng (曾生跃)[1], Xiaojun Xu (许晓军)[1,2,3], and Chaofan Zhang (张超凡)[1,4*]

[1] College of Advanced Interdisciplinary Studies, National University of Defense Technology, Changsha 410073, China

[2] State Key Laboratory of Pulsed Power Laser Technology, Changsha 410073, China

[3] Hunan Provincial Key Laboratory of High Energy Laser Technology, Changsha 410073, China

[4] Nanhu Laser Laboratory, National University of Defense Technology, Changsha 410073, China

*Corresponding author: c.zhang@nudt.edu.cn

Received August 25, 2022 | Accepted April 4, 2023 | Posted Online June 5, 2023

Photoelectron spectroscopy is a powerful tool in characterizing the electronic structure of materials. To investigate the specific region of interest with high probing efficiency, in this work we propose a compact *in situ* microscope to assist photoelectron spectroscopy. The configuration of long objective distance of 200 mm with two-mirror reflection has been introduced. Large magnification of 5 × to 100 ×, lateral resolution of 4.08 μm, and longitudinal resolution of 4.49 μm have been achieved. Meanwhile, the testing result shows larger focal depth of this *in situ* optical microscope. Similar configurations could also be applied to other electronic microscopes to improve their probing capability.

Keywords: photoelectron spectroscopy; *in situ* optical microscope; long objective distance; large magnification.
DOI: 10.3788/COL202321.061101

1. Introduction

Photoelectron spectroscopy is a powerful tool in direct investigation of the electronic structure of materials. The requirement of photoelectron spectroscopy with spatial resolution has become urgent both in scientific research and industry applications[1–7]. However, the processes of scanning the whole sample and especially targeting the specific region of interest are usually very time-consuming. An assisting *in situ* microscope could significantly improve probing efficiency. Similar inconvenience also exists in other types of electronic microscopes, including the scanning electron microscope (SEM)[8], the transmission electron microscope (TEM)[9–11], the scanning tunneling microscope (STM)[12], tip-enhanced Raman spectroscopy (TERS)[13], and photoemission electronic microscopy (PEEM)[14]. Several methods have been tried to solve this problem. As for the spatial and angular-resolved photoemission spectroscopy (sr-ARPES), by now only one system (the end station at the Elettra synchrotron in Italy)[15–17] with an assisting optical microscope has been reported, utilizing a homemade miniature photoelectron analyzer and telescopic optical structure, the configuration of which makes the direct view of microscopy possible. Unfortunately, it is not real *in situ* but side assisting. In the other setups of electronic microscopy, the most common method currently used is to have a conventional microscope adhere the windows of the experimental vacuum chamber. This poses some obstacles to the operation and causes a limitation of magnification. To the best of our knowledge, the scheme of an *in situ* microscope simultaneously implementing photoelectron spectroscopy is still lacking.

The design and realization of the *in situ* optical microscope for photoelectron spectroscopy may face many difficulties. First, to realize *in situ* monitoring of samples, the components of the optical microscope need to keep away from the head of the photoelectron analyzer that directly faces the sample surface, with only few centimeters in between. Second, since the direct microscope on top is not possible, the new configuration design should naturally consider the idea of bending the optical path, due to the limited space in an ultrahigh vacuum (UHV) chamber. The objective lenses have to be mounted away from the sample area, which results in a distance of at least 100 mm from the sample to the objective lens, making the realization of high resolution and large magnification difficult.

In this paper, we report a compact *in situ* microscope for photoelectron spectroscopy as a side-assisting optical system inside a UHV chamber. The microscope is designed with a macro lens instead of an objective lens, achieving the best spatial resolution and 1:1 magnification at a long objective distance of 200 mm. Two-mirror reflection is employed to guide the optical path from the sample surface to the macro lens. In this configuration,

there is no optical component mounted directly over the surface of the sample, thus avoiding the blocking of the emitting photoelectrons of the sample to the electronic energy analyzer. A microscope is installed downstream from the optical path to achieve a large magnification. Combined with the microscopic lens group and macro lens, the total optical magnification of 5 × to 100 × has been realized. The compact design enables integration into most commercial photoelectron spectroscopy and makes *in situ* probing possible. According to the testing results of the various patterns, the lateral resolution reaches 4.08 μm, and the longitudinal resolution achieves 4.49 μm. The impact of curvature only makes a 0.5 μm resolution reduction in the fringe, and distortion could be controlled to less than −0.39% in the lateral direction and −0.77% in the longitudinal direction. Moreover, the larger focal depth could be clearly observed by comparing it with the result of a conventional optical microscope.

2. Methods

Figure 1 illustrates the schematic drawing of the system we propose, which contains three functional parts: an LED collimation stage, an ultrahigh vacuum chamber, and a microscopic imaging part. The observation path and the sample are placed in parallel. In this way, other detectors or probing means can be applied directly above the sample.

As the standard UHV testing chamber shows, a photoelectron analyzer is placed directly above the sample, and the distance from its extreme end to the specimen is only 35 mm. This avoids the microscope blocking the photoelectron collection of the analyzer and setting the reflected light receiving configuration away from the main photon-in-electron-out path is necessary. In addition, considering the very limited space in a vacuum chamber, we only set two mirrors to transmit the reflected light out of the sample-analyzer area. The illumination light, mounted outside the UHV, with a center wavelength of 620 nm from a red LED (Daheng Optics, GCI-060401) is first collimated by a lens L1 (Foctek Photonics, C-M35-1F12) to form a virtually 0.5-mm-diameter wide beam. After passing through the vacuum window, the light source is defocused onto the specimen. The beam is reflected off the sample, consequently passes through two mirrors, M1 and M2, and then goes into microscopic imaging part, which is fixed on a five-axis motorized stage. Subsequently, the reflected light passes through a macro lens that is set to converge the light and compensate for tilt error. The obtained image plane (IP) is located at the front focal plane of the objective lens (Olympus). Combined with tube lens (Olympus, SWTLU-C) to realize infinite observation, the objective lens can be replaced with a different numerical aperture (NA) to achieve various magnification. The tube lens finally forms the image on the sensor of a low-noise and high dynamic range CMOS camera (Phenix, MC-DK20U(C)-TP).

In order to ensure that the microscopic imaging part is sitting away from the electronic analyzer, a long object distance of at least 200 mm is required. However, the object distances of traditional telephoto lenses are generally less than 100 mm, which limits the choice of objective lens with large NA. We therefore use a macro lens (Canon, EF 100 mm *f*/2.8 IS USM) as a special kind of imaging lens, which not only meets the demand of object distance, but can achieve the 1× magnification at the closest focusing distance of 300 mm (the minimum magnification is 0.5×). Equipped with different objective lenses (10× to 100×), the compact *in situ* microscope for photoelectron spectroscopy can achieve a total optical magnification of 5–100 times. Furthermore, to compensate for the image plane tilt caused by lateral illumination, an actively tilted CMOS camera is assigned (the tilt angle is determined by the Scheimpflug principle[18]).

3. Experimental Results

To evaluate the imaging quality of our compact *in situ* optical microscope, a combined test target (Lbtek, RTR1Ee) suitable for multiple tests with a United States Air Force (USAF) resolution test target (six groups with six element sizes), a grid pattern of 100 μm, and a group of variable line gratings (1.25 lp/mm to 250 lp/mm) were used. In this experiment, the objective lens with magnification of 40× (Olympus, UPLXAPO) was configured. First, to measure the resolution limit of the system, we imaged groups 6 and 7 of the USAF target; the result is shown in Fig. 2(a). It can be seen that the geometric shape and relative position of the stripes belonging to group 6 and group 7 of

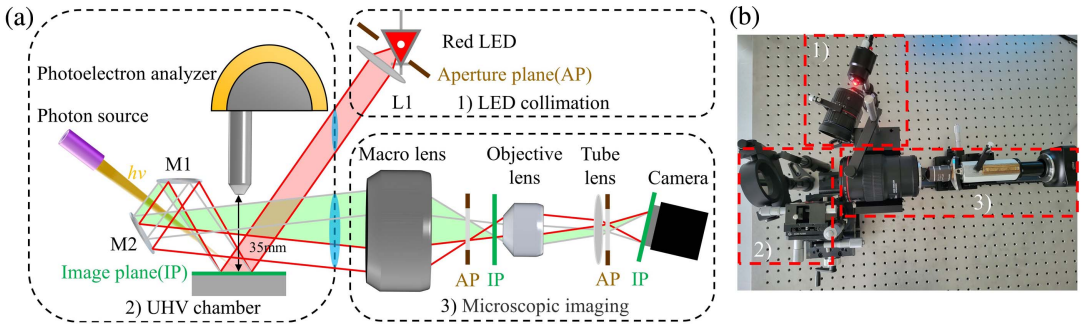

Fig. 1. Principle and scheme of the side-assisting microscope. (a) Principal optical setup including three parts: (1) LED collimation stage; (2) ultrahigh vacuum chamber; (3) microscopic imaging. (b) Photo of the experimental setup in a clean laboratory air environment.

element 1 (128 lp/mm) could be observed clearly by the system, representing the resolution obtained at least 7.8 μm in this way. Subsequently, the part in the white outlined region of the USAF was selected as the middle observation area, where the zooming-in image with a smaller field of view (FOV) is shown in Fig. 2(b). Targeting and resolving this area could accurately quantify the spatial resolution of our microscope. The spatial resolution was measured by a standard knife-edge scan. Considering the side illumination and distant object distance in our system, the edge spread function (ESF) is estimated by plotting the intensity distributions via the two blue lines, investigating differences between lateral (X) and longitudinal (Y) directions. As shown in Figs. 2(c) and 2(d), the line spread function (LSF), the first derivative of ESF, results in the full width at half-maximum (FWHM) of 6.29 μm in the direction of X and 6.69 μm in the direction of Y, indicating a better limit of resolution in the lateral direction. The resolution of the measurement here can be slightly better than the result in Fig. 2(a). This is probably caused by the field curvature of the microscope, which leads to the lower resolution of the edge position than that of the center.

To characterize the possible field curvature of the system, we next selected vertically oriented grating (50 lp/mm) with a 10 μm step size. The result is shown in Fig. 3(a), where the microscopic image is provided in the insets as references. From the image in Fig. 3(a), a line cut of intensity distribution across the lines is taken and shown in Fig. 3(b), clearly showing the expected period of 20 μm. Then, the derivative of the line cut intensity with respect to longitudinal position is used to measure the difference of resolution between the central and fringe FOVs. As the derivative (red line) in Fig. 3(b) shows, each peak represents the LSF of the upper edge of a bright stripe, whereas each trough represents the LSF of the bottom edge, resulting in the different

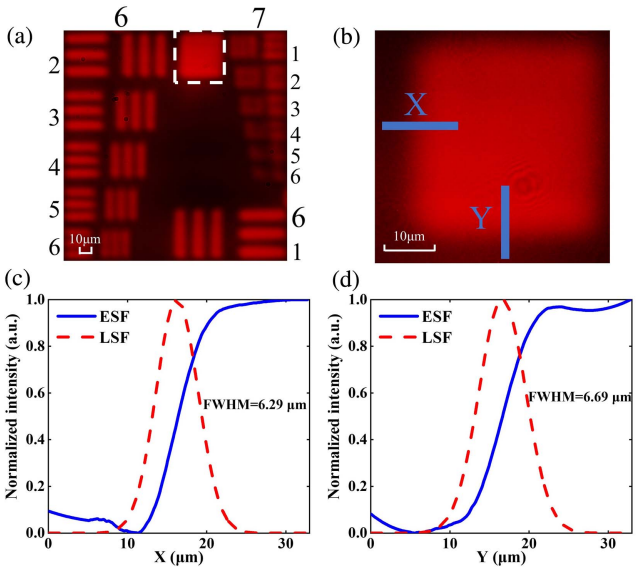

Fig. 2. System spatial resolution testing. (a) Image of a USAF target (groups 6 and 7); (b) region for experimenting; (c) and (d) assessed resolution of the side-assisting microscope system along the solid line (X and Y) of (b), respectively.

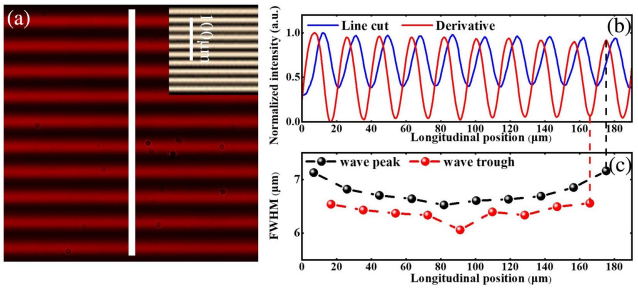

Fig. 3. System field curvature testing. (a) Two-dimensional image of a 20 μm-period grating with a vertical orientation. The inset in (a) shows a microscopic image of the grating. (b) The intensity profile (blue line) extracted along the white solid line in (a) and the first derivative of the line cut (red line); (c) FWHM corresponding to the peaks (black line) and troughs (red line) of the first derivatives of the intensity in (b).

FWHM shown in Fig. 3(c). It is obvious that the FWHM of the wave peak is generally larger than the corresponding trough, which means the resolution of the bottom edge is better than that of the upper edge. We attempted to interpret this phenomenon. The combined resolution plate has a certain thickness and only the test pattern is coated with Cr, which causes the illumination light to pass through in the remaining positions. Since our system uses sideways illumination, the light may be reflected many times in the backward direction of the target and transmitted from one side, resulting in a false image on that side and thus reducing the resolution. In addition, it can be clearly seen that the FWHM at the middle of the image is significantly lower than that at the edge. The maximum difference is only 0.5 μm, indicating that the resolution of the center is slightly better than that of the edge, both in upper and bottom areas. The result shows that a certain field curvature exists in the system, leading to the decrease in resolution in the edge position. However, the resolution reduction of 0.5 μm has little effect on the side-assisting observation of wide FOV in photoelectron spectroscopy, which benefits from the correction of the Scheimpflug principle, confirming our microscope can well provide *in situ* optical observation.

Considering that the purpose of our system is to assist the photoelectron spectroscopy to probe the whole area of interest, the image field distortion of the microscope is required to be controlled to a small level to ensure the accuracy of localization. To quantify the degree of distortion, a standard grid pattern of 100 μm [Fig. 4(a)] was placed within the view. The result is shown in Fig. 4(b), which includes 16 complete grid patterns. Using the standard grid in Fig. 4(a) as a reference, the intensity curves are plotted in Figs. 4(c) and 4(d) along the horizontal and vertical yellow solid lines in Fig. 4(a), respectively. The same approach is applied to the resulting intensity curves. In comparison with the intensity profiles of the standard grid and the result, it is observed that the peak positions of both are almost identical. Since our work is concerned with the relative position of the feature in the sample and the aberration only changes the position of the off-axis object point on the ideal surface, no distortion can

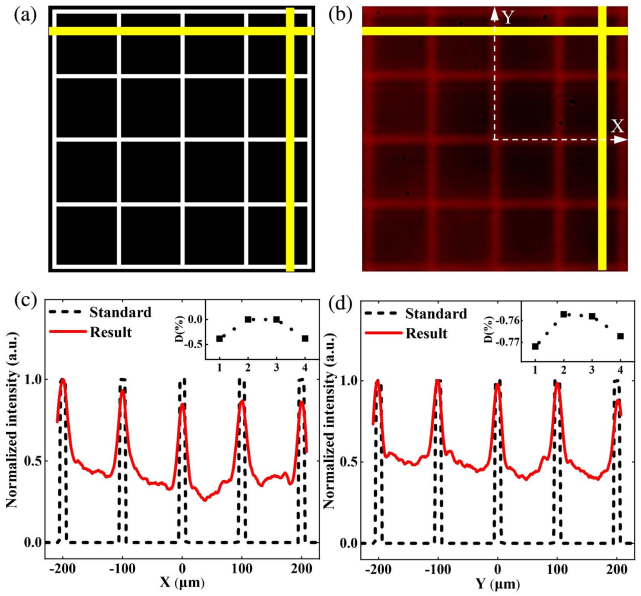

Fig. 4. System distortion testing. (a) Standard grid pattern of 100 μm; (b) experimental result of standard grid pattern; (c) intensity profiles of standard grid (black lines) and experimental result (red lines) plotted via the horizontal yellow solid lines in (a) and (b); (d) intensity profiles of standard grid and experimental result plotted via the vertical yellow solid lines in (a) and (b); insets in (c) and (d) show the distortion of *X* direction and *Y* direction, respectively.

be observed in the two axes orthogonal to each other at the center in Fig. 4(b). Thus, the distortion can be defined as

$$D = \frac{z_0 - z_P}{z_0}, \tag{1}$$

where z_0 is the distance from the extreme point to the axis without distortion and z_P is the distance from the extreme point of the experimental result to the axis. As the insets in Figs. 4(c) and 4(d) show, the field distortion of the lines are compared with the center line; we note that 1, 2 are for the left (upper) lines and 3, 4 are for the right (lower) lines. Results show the maximum aberration is controlled within −0.39% in the lateral direction and −0.77% in the longitudinal direction. The reason for the large longitudinal aberration may be artifacts caused by light returning from the bottom of the resolution target. These results confirm that our system has precise auxiliary positioning capability within a large FOV of 400 mm.

To further validate the imaging feasibility of the system in actual material sample, a device was prepared with a specific gold electrode pattern of parallel microline structures. The image of the device is provided in Fig. 5(a) as a reference; it has an overall size of 1.5 mm × 1.5 mm with the gold-plated white area and the blue area of silicon dioxide substrate. The part in the red outlined region of the sample is selected as the target area, where the zooming-in image is shown in the right-hand area, indicated by the dotted line. Targeting and resolving these areas could well reflect the performance of our microscope.

First, the optical resolution of our setup in the material sample experiment is evaluated by plotting the intensity profiles via the line cuts obtained from Fig. 5(d), both in the directions of *X* and *Y*. As can be expected, the space limitation directly above the sample causes the illumination light to be obliquely incident, making a lower vertical resolution rather than a horizontal; a similar phenomenon can be seen in the testing of combined targets. Indeed, as shown in Figs. 5(e) and 5(f), the resolution measured along the two axes is slightly different, being 4.08 μm along the direction perpendicular to the incident plane, and 4.49 μm along the direction parallel to it. It is noteworthy that the resolution measured in the sample experiment was improved by about 2 μm, compared to the result of the resolution plate. This may be due to the tiny thickness of the material sample, resulting in little effect on the reflected light from the bottom, the condition readily available in photoelectron spectroscopy and other electronic microscopes (the thickness is typical only in the hundred nanometer range).

As Fig. 5(e) demonstrates, the stripes with 10 μm interval can be clearly distinguished by the system and no obvious field curvature or distortion exists at the edge of the FOV. Furthermore, in comparison with the result of the same area

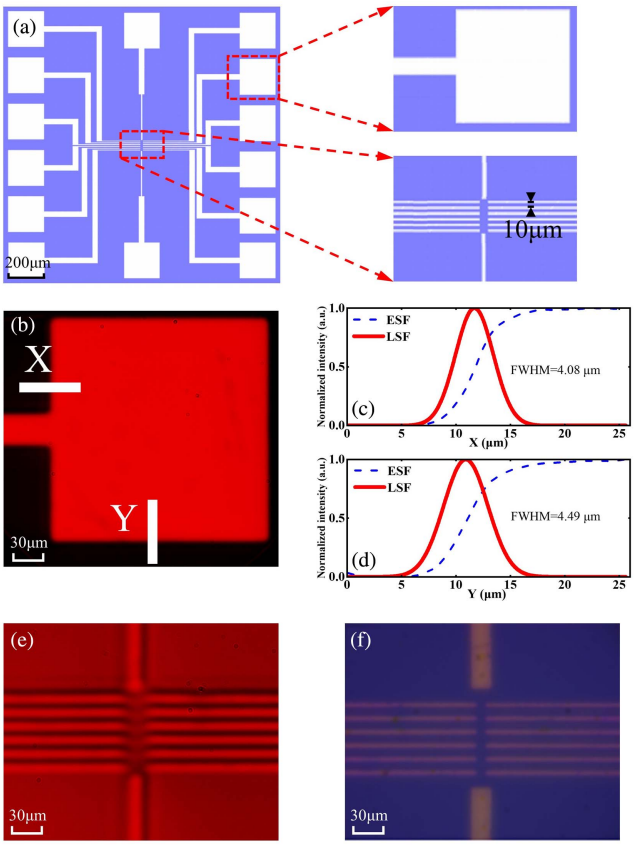

Fig. 5. Experimental results and quantitative analysis. (a) Sample morphology and region for experimenting; (b) result of square-shaped area; (c) and (d) resolution measured along the two line cuts in (b), respectively; (e) result of central stripe area with our setup; (f) result of conventional high-resolution optical microscope at 40×.

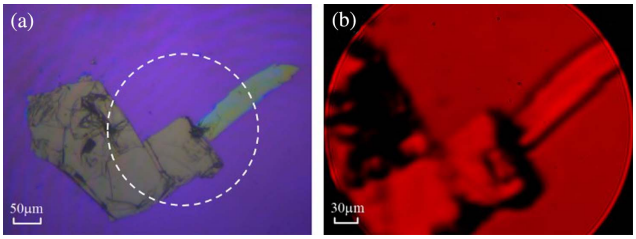

Fig. 6. Microscope images of graphene flake. (a) Conventional optical microscope image of the sample at 25×; (b) microscope image with the proposed setup.

under conventional optical microscope at 40× displayed in Fig. 5(f), the gold-plated electrode parts are higher than the silicon dioxide area, and a height difference between the center part and the edge of the gold-plated area could be clearly observed in our system, indicating that our microscope has a large depth of field, which is impossible to observe with other conventional optical microscopes. To verify the practice performance of the system, a graphene flake is also tested. The image in Fig. 6(b) not only captures the shape of the graphene flake in Fig. 6(a) but also vividly reveals the stereomorphology of the sample, which we assume was caused by the small tilt angle between the position of the mirror and the sample holder. Fortunately, the unexpected 3D features appearing in the image are merits of the system from the side of the potential users of photoelectron spectroscopy.

4. Conclusion

In summary, we have designed and built a compact *in situ* microscope for photoelectron spectroscopy, solving the problem of the inconformity for mounting an *in situ* microscope and the difficulty of samples to zoom in with a large magnification. The observation path of our microscope in this paper and the sample in UHV are placed in parallel, avoiding obstructing other detectors from observing directly over the sample. We used the macro lens to replace the objective lens in the conventional optical microscope, achieving a 1:1 magnification at a long object distance of 200 mm. Combined with the microscope lens group, we achieved a maximum magnification of 100 times. The long object distance can satisfy the configuration of most photoelectron spectroscopy and other electronic microscopies, making the microscopic imaging part of our system mounted away from the main probing means. Even though a few setups may require a longer object distance, it can be achieved by adjusting the macro lens, though it will lose some resolution and magnification. According to the experimental results, the lateral resolution can reach 4.08 μm, and the longitudinal resolution can achieve 4.49 μm. The impact of curvature only makes a 0.5 μm resolution reduction in the edge, and distortion could be controlled to a small level, to less than −0.39% in the lateral direction and −0.77% in the longitudinal direction. The larger focal depth can also assist other electron microscopes in probing uneven samples. A practice test performed on the graphene flake verifies the feasibility of the proposed configuration in the studies of photoelectron spectroscopy and other related microscope systems.

Acknowledgement

This work was supported by the National Natural Science Foundation of China (No. 11774427). We thank the staff of ShanghaiTech University for their technical support and assistance in designing.

References

1. H. Yuan, Z. Liu, G. Xu, B. Zhou, S. Wu, D. Dumcenco, K. Yan, Y. Zhang, S. K. Mo, and P. Dudin, "Evolution of the valley position in bulk transition-metal chalcogenides and their monolayer limit," Nano Lett. **16**, 4738 (2016).
2. H. Peng, N. B. M. Schroter, J. Yin, H. Wang, T. F. Chung, H. Yang, S. Ekahana, Z. Liu, J. Jiang, and L. Yang, "Substrate doping effect and unusually large angle van Hove singularity evolution in twisted bi- and multilayer graphene," Adv. Mater. **29**, 1606741 (2017).
3. H. Yang, A. Liang, C. Chen, C. Zhang, N. Schroeter, and Y. Chen, "Visualizing electronic structures of quantum materials by angle-resolved photoemission spectroscopy," Nat. Rev. Mater. **3**, 341 (2018).
4. Y. J. Chen, L. X. Xu, J. H. Li, Y. W. Li, H. Y. Wang, C. F. Zhang, H. Li, Y. Wu, A. J. Liang, C. Chen, S. W. Jung, C. Cacho, Y. H. Mao, S. Liu, M. X. Wang, Y. F. Guo, Y. Xu, Z. K. Liu, L. X. Yang, and Y. L. Chen, "Topological electronic structure and its temperature evolution in antiferromagnetic topological insulator $MnBi_2Te_4$," Phys. Rev. X **9**, 041040 (2019).
5. C. Zhang, Y. Li, D. Pei, Z. Liu, and Y. Chen, "Angle-resolved photoemission spectroscopy study of topological quantum materials," Annu. Rev. Mater. Res. **50**, 131 (2020).
6. Y. W. Li, H. J. Zheng, Y. Q. Fang, D. Q. Zhang, and Y. L. Chen, "Observation of topological superconductivity in a stoichiometric transition metal dichalcogenide 2M-WS_2," Nat. Commun. **12**, 2874 (2021).
7. Y. Mao, D. Zhao, S. Yan, H. Zhang, and Y. Chen, "A vacuum ultraviolet laser with a submicrometer spot for spatially resolved photoemission spectroscopy," Light Sci. Appl. **10**, 22 (2021).
8. J. Zach and M. Haider, "Correction of spherical and chromatic aberration in a low voltage SEM," Optik **98**, 112 (1995).
9. J. Yi, C. Zhen, Y. Han, D. Pratiti, G. Hui, S. Xie, P. Prafull, M. W. Tate, P. Jiwoong, and S. M. Gruner, "Electron ptychography of 2D materials to deep sub-angstrom resolution," Nature **559**, 343 (2018).
10. G. Hansmann and H. Pietsch, "Elektronenmikroskopische Abbildung von Membranfilteroberflächen," Naturwissenschaften **36**, 250 (1949).
11. A. H. Zewail, "Four-dimensional electron microscopy," Science **328**, 187 (2010).
12. S. Park and C. F. Quate, "Scanning tunneling microscope," Rev. Sci. Instrum. **58**, 2010 (1987).
13. V. Deckert, "Tip-enhanced Raman spectroscopy," J. Raman Spectrosc. **40**, 1336 (2010).
14. L. Douillard, F. Charra, Z. Korczak, R. Bachelot, S. Kostcheev, G. Lerondel, P. M. Adam, and P. Royer, "Short range plasmon resonators probed by photoemission electron microscopy," Nano Lett. **8**, 935 (2008).
15. S.-K. Mo, "Angle-resolved photoemission spectroscopy for the study of two-dimensional materials," Nano Converg. **4**, 6 (2017).
16. J. Avila and M. C. Asensio, "First NanoARPES user facility available at SOLEIL: an innovative and powerful tool for studying advanced materials," Synchrotron Radiat. News **27**, 24 (2014).
17. C. Wiemann, M. Patt, I. P. Krug, N. B. Weber, and C. M. Schneider, "A new nanospectroscopy tool with synchrotron radiation: NanoESCA@Elettra," e-J. Surf. Sci. Nanotech. **9**, 395 (2011).
18. M. Corbett, N. Maycock, E. Rosen, and D. O'Brart, "Scheimpflug camera-based systems," in *Corneal Topography: Principles and Applications* (Springer International Publishing, 2019), p. 43.